ISSN 1029-9599, Physical Mesomechanics, 2022, Vol. 25, No. 5, pp. 466–478. © Pleiades Publishing, Ltd., 2022.
Russian Text © The Author(s), 2022, published in Fizicheskaya Mezomekhanika, 2022, Vol. 25, No. 3, pp. 98–112.

Mesoeffect of the Dual Mechanism of Hydrogen-Induced Cracking

V. A. Polyanskiy[1]*, A. K. Belyaev[1], Yu. S. Sedova[1], and Yu. A. Yakovlev[1]

[1] *Institute for Problems in Mechanical Engineering, Russian Academy of Sciences, Saint Petersburg, 199178 Russia*
** e-mail: vapol@mail.ru*

Received February 18, 2022; revised May 23, 2022; accepted May 23, 2022

Abstract—One of the main methods of protecting pipelines and machine parts against stress corrosion and hydrogen embrittlement is to test metals for hydrogen-induced cracking. The hydrogen-induced cracking test is a standard procedure for testing steels and titanium alloys and for studying hydrogen resistance. The experimentally revealed phenomenon of nonuniform hydrogen distribution after hydrogen charging of specimens is called the skin effect. Here we study the influence of the skin effect after hydrogen charging on the crack growth under mechanical stresses and the influence of a 50-μm-thick skin layer on the durability of bulk specimens. A corset-type cylindrical specimen with a circumferential notch is considered. The Oriani decohesion model is chosen as a hydrogen embrittlement model. The investigation is performed using our data on the real nonuniform hydrogen distribution and the literature data on hydrogen diffusion coefficients, diffusion activation energy, steel parameters, cohesive law parameters, as well as other parameters of the hydrogen embrittlement model proposed by Serebrinsky. Hydrogen redistribution is described by the diffusion law taking into account mechanical stresses. Modeling is carried out with the original finite volume code in the axisymmetric setting. Crack propagation parameters are determined. The fracture pattern is complex. Cracking first occurs by the hydrogen-enhanced decohesion mechanism and then by the conventional mechanism, which explains the experimentally observed brittle-ductile fracture behavior in tensile hydrogen-charged specimens.

Keywords: hydrogen-induced cracking test, skin effect, decohesion, hydrogen-charged specimen, fracture

DOI: 10.1134/S1029959922050095

1. INTRODUCTION

Engineering practice is constantly faced with the problems of hydrogen-induced cracking (HIC), hydrogen embrittlement, stress-corrosion cracking, and hydrogen damage. This is explained by the fact that hydrogen is widely spread in nature, either in a gaseous state or in the form of chemical compounds, water being the most widespread. For example, the oil and gas industry deals with these phenomena in all types of corrosion [1].

As a rule, an increase in the strength of metals and alloys is accompanied by a decrease in plasticity. Unlike other alloy components with the maximum permissible concentration of hundredths and thousandths of a percent, hydrogen begins to influence the properties of some metals at the mass concentration of one hundred thousandths of a percent.

Therefore, there is a special sensitivity of modern high-strength alloys with iron, aluminum, magnesium or nickel matrices to low concentrations of hydrogen. For Bessemer steels, the maximum permissible mass concentration of hydrogen is about 4 ppm, while, for modern ultrahigh-strength steels, it is about 30 times less.

Even if such low hydrogen concentrations are achieved in the production of alloys, the subsequent processing and operation of metal parts will increase the concentration of hydrogen and its significant influence on the mechanical properties of metals and alloys, which are strength, ductility, fracture toughness, and crack resistance [2].

The problem of the interaction of metals with hydrogen used as an energy source in various hydrogen energy projects is worthy of notice. Transportation of mixtures of natural gas and hydrogen [3–7] leads to a decrease in the ductility, fracture toughness, and crack resistance of steel walls of pipelines [8–11], to say nothing of the transportation of pure hydrogen gas [9, 12].

Thus, the influence of hydrogen on the properties of materials cannot be left disregarded without serious consequences. Solving engineering problems requires that the effect of hydrogen on the strength of materials be evaluated at the design stage of structures and during their operation.

Tests on hydrogen-charged notched corset metal specimens for strength, fatigue strength, ductility, and fracture toughness are often used in engineering practice and in research. Such tests allow the quality control of metals and the selection of metals that are resistant to hydrogen embrittlement and hydrogen-induced cracking.

Hydrogen charging is a standard procedure for HIC testing of steels for pipelines and other elements of machines [13–16]. In this case, use is usually made of nongaseous methods of hydrogen saturation [14, 16], which always lead to the formation of a skin layer for the time recommended by the saturation standards.

High inhomogeneity of distribution of hydrogen concentrations after the standard saturation procedure was reported in [17–20]. This phenomenon was referred to as the skin effect [17, 19]. Due to this effect, the hydrogen concentration in the surface layer with the approximately one grain thickness (10–100 μm) can exceed the concentration inside the specimen by tens of times. Modeling of this phenomenon has so far been carried out without taking into account the influence of the skin effect on the fracture of metal specimens [21].

The skin layer is sometimes explained by the very slow diffusion of hydrogen [22, 23]. However, previously we discussed in detail the experimental results that do not confirm this assumption [19]. In any case, a large increase in the hydrogen concentration in the boundary layer of metals is of fundamental importance to the test results.

The effect of the skin layer on the results of mechanical tests on hydrogen-charged specimens also has not been investigated. It follows from practice that standard methods for hydrogen saturation lead to a strong decrease in plasticity (relative to residual elongation) and strength of the entire specimen. At the same time, fracture often has a dual pattern: the fracture surface of the specimen has areas of both hydrogen brittleness and ductile fracture [24, 25].

Correct consideration for the influence of the skin layer is very important when modeling hydrogen embrittlement. This is due to the need of understanding the leading mechanisms of fracture and predicting the destruction of machine parts operating in aggressive media.

Crack resistance is critically reduced by hydrogen; therefore, the two most popular and well-known calculation models of hydrogen brittleness (hydrogen-enhanced decohesion (HEDE) [26] and hydrogen-enhanced localized plasticity (HELP) [27, 28]) are based on the approaches of crack theory and consider the nucleation and sink of dislocations at the crack tip as the physical mechanism of fracture. The initially developed models significantly differed from each other. Thus, the HEDE model considered brittle fracture as a result of the development of hydrogen embrittlement without plastic deformation, while, on the contrary, the HELP model interpreted the effect of hydrogen dissolved in a metal as the action of a chemical constituent, which reduces the energy required for dislocation nucleation. By the HELP mechanism, hydrogen is concentrated under the action of internal stresses at the crack tip, where metal "softening" or localized plasticity occurs.

These models were verified in numerous experiments [29–35] (see also reviews [24, 25, 36, 37]). The bulk of the experimental results were obtained on specimens artificially charged with hydrogen in the electrolyte solution, as a rule, using cathodic charging.

The investigations showed that the fracture surfaces of experimental specimens have not only areas of hydrogen brittleness but also zones of ordinary fracture without pronounced hydrogen signs. The idea of the hybrid HELP + HEDE mechanism was proposed for explaining this dual fracture pattern [38–41] (a review is done in [24]).

The HELP and HEDE models can be formally combined within the Abaqus package. The HELP method can be used to describe plastic flow at low local hydrogen concentrations, and the HEDE method can be employed to analyze the crack propagation from the groove or notch in the specimen at local hydrogen concentrations above the switching threshold of the models. This was done for the two-dimensional case in [42]. The combined model was applied to determine the fatigue crack growth rate with the parameters given in advance. The authors pointed to the existing problems of determination of a large number of parameters and stated only a qualitative agreement between the simulation results and the experimental findings.

The combined model with additional consideration for the void formation under loading was used to

simulate the crack growth in a notched viscoelastic material in [43]. In this case, the transport of hydrogen is modeled by the simplified method [44], and the cohesive law is independent of hydrogen. The problem of crack growth in high-strength chromium steel 690 around an inclusion was studied in [45–47]. The HELP model in the form of [44] is supplemented by the HEDE cohesive law.

In all of the above works, the authors assume the uniform hydrogen concentration in metal specimens after hydrogen charging. All changes in the hydrogen concentration are associated with its redistribution under an external load or during the crack growth. As a rule, a specific value of the initial hydrogen concentration results from fitting the model parameters to the experimental data. Therefore, it varies within a wide range from 0.0005 [48] to 1.5 ppm in various papers [49].

By comparing the initial HELP and HEDE approaches, we can conclude that the HEDE mechanism corresponds to the concept of brittle fracture, which is observed in steels at high hydrogen concentrations [42]. Therefore, the use of the HEDE mechanism in describing the consequences of the skin effect for the crack growth should provide an adequate model for fracture of specimens artificially saturated with hydrogen in electrolyte solutions or at cathodic charging.

2. ORIANI DECOHESION MODEL OF BRITTLE FRACTURE

The process of hydrogen transport inside a solid is traditionally considered within the HEDE model as a diffusion process. It is described within Fick's law with the additional term that takes into account the thermodynamic (or chemical) potential V [50]:

$$\frac{\partial C}{\partial t} = \nabla \cdot \left[D(T, \mathbf{r}) \left(\nabla C + \frac{C \nabla V}{RT} \right) \right]. \qquad (1)$$

Here C is the hydrogen concentration, D is the diffusion coefficient, R is the gas constant, T is the absolute temperature, r is the position vector, t is the time, and ∇ is the Hamilton nabla operator. Taking into account the action of mechanical stresses, this equation can be rewritten as

$$\frac{\partial C}{\partial t} = D[T]\nabla^2 C - D[T]\frac{V_{\mathrm{H}} \nabla C \cdot \nabla \sigma}{RT} - D[T]\frac{C V_{\mathrm{H}} \nabla^2 \sigma}{RT}, \qquad (2)$$

where σ is the primary stress (spherical part of the stress tensor), and V_{H} is the partial molar volume of hydrogen.

Then, the fracture criterion associated with the magnitude of crack opening comes into operation within the HEDE mechanism. According to Gorsky's law [51], hydrogen is concentrated in the region of the maximum stress tensor (i.e. spherical part of the stress tensor) and reduces the adhesion of the crack faces which leads to decohesion [26].

These changes in cohesive forces between grains are described through the parameter of coverage of the free surface of a crack with hydrogen atoms θ, which can be represented as [52]

$$\theta = \frac{C}{C + \exp[-\Delta g_{\mathrm{H}}/(RT)]}, \qquad (3)$$

where Δg_{H} is the Gibbs free energy difference between hydrogen adsorbed inside the crystal lattice and at the crystal boundary (taken from the experiment). Formula (3) was obtained by Serebrinsky [52] by comparing the parameters of hydrogen trapping in the metal based on the McLean ratio [53].

A value of the parameter θ determines the change in the specific energy of the free surface $\gamma(\theta)$, which depends on the surface sorption of hydrogen [52]:

$$\gamma(\theta) = (1 - 1.0467\theta + 0.1687\theta^2)\gamma(0). \qquad (4)$$

This dependence was obtained by approximating the graph for the case of deformation of a pure Fe single-crystal saturated with hydrogen in the (110) crystallographic direction.

From the energy identity $2\gamma(\theta) = \sigma_{zc}(\theta)\delta_c(\theta)$, where $\sigma_{zc}(\theta)$ is the maximum cohesive stress normal to the crack edges, and $\delta_c(\theta)$ is the maximum possible crack-opening displacement without breaking bonds (decohesion), the law of hydrogen-induced degradation has the form [52]

$$\sigma_z(\theta) = (1 - 1.0467\theta + 0.1687\theta^2)\sigma_z(0) \qquad (5)$$

under the assumption of the weak dependence of the $\delta_c(\theta)$ value on the parameter θ.

In this paper, we investigate the applicability of the HEDE model to the description of hydrogen-induced fracture of a corset specimen with consideration for the skin effect.

3. INITIAL AND BOUNDARY CONDITIONS, MODEL PARAMETERS, AND CALCULATION PROCEDURE

We simulate uniaxial loading of a cylindrical specimen (Fig. 1) with the diameter $d = 10$ mm, which

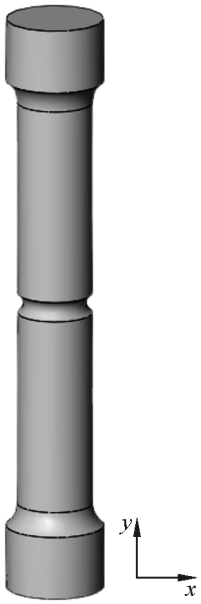

Fig. 1. Cylindrical specimen.

has a stress concentrator in the form of a semicircular groove with the radius $r = 0.5$ mm.

The problem is solved in the two-dimensional axisymmetric formulation. By symmetry, only a quarter of the cylinder is considered and a rectilinear structured grid consisting of triangles is generated. Thus, we model a sector of the longitudinal section of the specimen (Fig. 2), with the O*y* axis along the left side of the computational domain, and the *Ox* axis along the lower side. For a smoother distribution of the calculated values and greater accuracy of calculations, partitioning into finite volumes of two types (with different directions of the diagonal of a structural element) is carried out.

Specimens under study are made of high-strength steel PSB1080 with the following physical properties: ultimate strength $\sigma_B = 1498$ MPa, yield stress $\sigma_y = 1276$ MPa, mass density $\rho = 7800$ kg/m^3, and shear modulus $G = 79.3$ GPa. In addition, the diffusion coefficient $D = 2.5 \times 10^{-11}$ m^2/s, the partial molar volume of hydrogen $V_H = 2 \times 10^{-6}$ m^3/mol [54], the Gibbs free energy difference for hydrogen adsorbed inside the crystal lattice and at the crystal boundary $\Delta g_H = 30$ kJ/mol [54], and the absolute temperature $T = 298$ K.

The initial distribution of hydrogen over the specimen is found as follows: the background uniform concentration $\tilde{c}_0 = 0.1$ ppm over the entire domain and the concentration in the surface layer with the one element thickness $d_H = 20$ μm, $c_0 = 10$ ppm. The initial concentration characterizes the experimentally observed hydrogen content in the hydrogen-charged specimens, which results from the skin effect (the enlarged fragment in Fig. 2).

By symmetry, displacements along *Ox* vanish for the left side and displacements along *Oy* vanish for the lower side. The tensile stress $\sigma = 450$ MPa is applied to the upper side of the domain and acts along axis *Oy*.

We investigate the uncoupled problem by the iterative method, as suggested by the original Oriani model. Based on the stress-strain characteristics of a

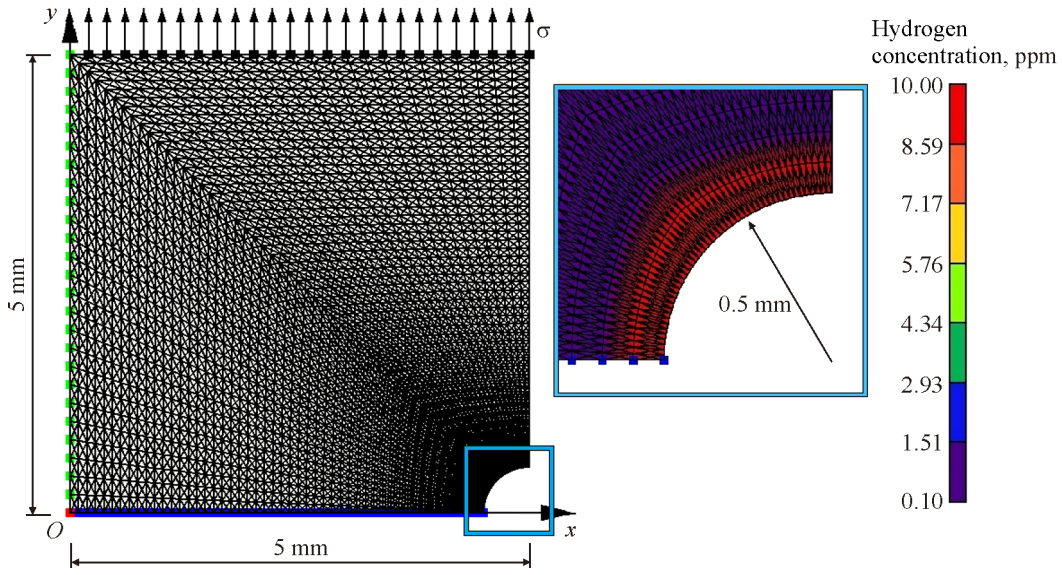

Fig. 2. Finite volume grid, boundary conditions (color online).

body, the diffusion problem of hydrogen redistribution over the specimen is solved. Then, the change in cohesive stresses (and consequently in the crack configuration) is calculated in terms of the hydrogen content in the domain and particularly near the crack tip. The hydrogen distribution has no direct effect on the stress state of a specimen.

The calculation procedure consists of two successive stages: (1) solving the mechanical problem of the stress-strain state of a specimen, and (2) analyzing the diffusion problem with the simultaneous calculation of cohesive stresses σ_z.

At the first stage, we obtain the numerical solution of the boundary-value problem of linear elasticity by means of the relaxation method proposed by Wilkins [55, 56]. It relies on the fact that the stationary problem is solved as the nonstationary problem, which is brought to the stationary mode.

The stress-strain state of the specimen obtained at this stage is transferred to the next stage. It includes the solution of the system of the foregoing equations (2), (3), (5):

$$\begin{cases} \dfrac{\partial C}{\partial t} = D[T]\nabla^2 C - D[T]\dfrac{V_{\mathrm{H}}\nabla C\cdot\nabla\sigma}{RT} \\ \qquad - D[T]\dfrac{CV_{\mathrm{H}}\nabla^2\sigma}{RT}, \\ \theta = \dfrac{55.85C\times10^{-6}}{55.85C\times10^{-6}+\exp[-\Delta g_{\mathrm{H}}/(RT)]}, \\ \sigma_z(\theta) = (1-1.0467\theta+0.1687\theta^2)\sigma_z(0). \end{cases} \tag{6}$$

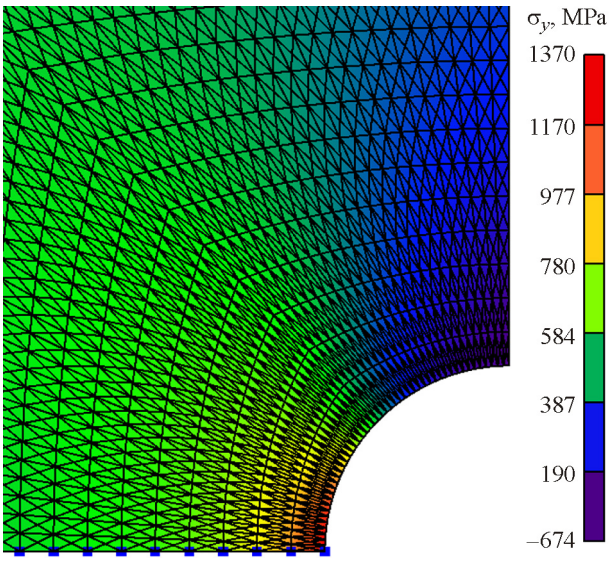

Fig. 3. Field of elastic stresses σ_y at the decohesion moment at the first node (color online).

The numerical solution of Eq. (2) is also carried out based on the relaxation method by Wilkins [55, 56]. The stress $\sigma_z(0)$ is taken to be $4.5\sigma_y$ according to [57].

The criterion of fracture, i.e. breaking of bonds between the atomic planes in the material, is fulfilled when the elastic stress obtained from the solution of the static problem exceeds the cohesive stress. As soon as this condition is fulfilled, the displacement constraint along axis *Oy* is removed at the grid node. This node is able to break away from the bottom face or, on account of symmetry, from the opposite node and to move upward under the action of tensile loads.

To monitor parameter changes during the problem solution and to reduce simulation errors, we use a well-tried approach [58–60]. To implement the approach, we developed a program code written in the Microsoft Visual Studio environment in C++ (VS), which allows obtaining a numerical solution to problems on the stress-strain state of a hydrogen-charged body within the finite volume method. Thus, we program the crack initiation and its propagation to a grid space. Thereafter a static problem is solved for the next crack propagation step, by repeating the calculation procedure.

4. SIMULATION RESULTS

The bond at the first grid node is broken instantly at the very first step of time integration due to high stresses acting near the stress concentrator and a significant hydrogen content in the surface layer. The field of distribution of the elastic stress component acting along the vertical axis near the groove at this time instant is shown in Fig. 3.

Maximum tensile stresses are seen to arise near the concentrator. The stress value for the first node along the crack propagation line is 1370.88 MPa.

Changes in the hydrogen concentration at this stage are insignificant. It decreases to $C = 9.99967$ ppm at the second node, and increases from the background value $C_0 = 0.1$ ppm to $C = 1.0028$ ppm at the third node.

A similar situation occurs for the second node along the crack propagation line. At the initial stages, the hydrogen content in the surface layer is so high that a crack initiates almost instantly by the HEDE mechanism.

The calculations for the third node show that the solution of the diffusion problem takes some time for hydrogen redistribution until it arrives at the actual concentrator, i.e. the supposed place of debonding

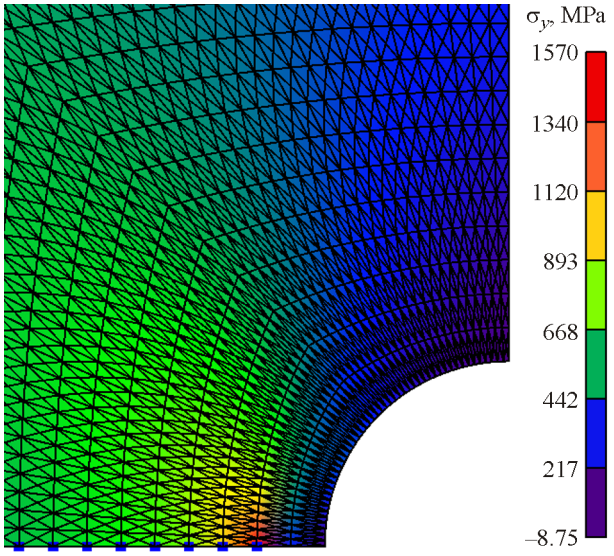

Fig. 4. Field of elastic stresses σ_y at the decohesion moment at the third node (color online).

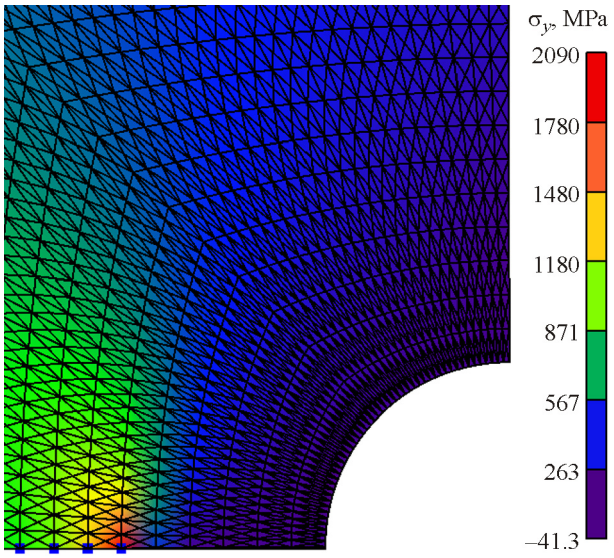

Fig. 6. Field of elastic stresses σ_y at the decohesion moment at the seventh node (color online).

between the atomic planes of the material. The calculated time of this process is $t = 9.17$ s, and the critical hydrogen concentration is $C = 0.386$ ppm. The distribution of the elastic stress component at the moment of fulfillment of the fracture criterion at the third node is shown in Fig. 4.

The tendency towards increasing the time interval between the fulfillment of the fracture criterion for two successive nodes persists at subsequent integration steps. The corresponding dependence is shown in Fig. 5.

Starting from the third node, diffusion takes more and more time for hydrogen redistribution and accumulation at the potential fracture site of the material. At the seventh node, which corresponds to the distance 0.551 mm from the groove edge, this time interval (from the moment the sixth node was detached) amounts to 122.85 s, and the critical concentration is $C = 0.213$ ppm. The resulting elastic stress field is shown in Fig. 6.

Thereafter, as seen from Fig. 5, the time between the fulfillment of the fracture criterion at the adjacent nodes begins to decrease gradually. This is due to an increase in the level of stresses acting near the concentrator. Due to a lower hydrogen content in the region, cohesive stresses become lower than elastic ones, which leads to the propagation of a crack to a grid space according to the established algorithm.

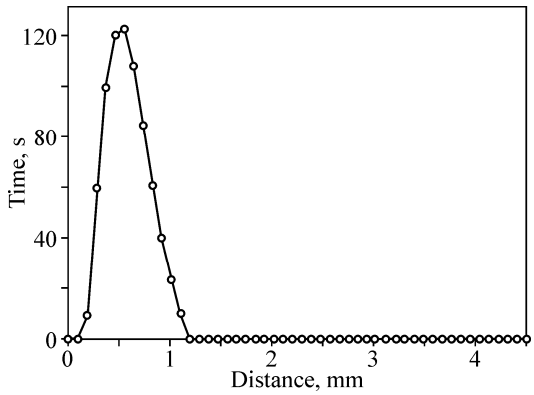

Fig. 5. Time between the fulfillment of the fracture criterion at the adjacent nodes.

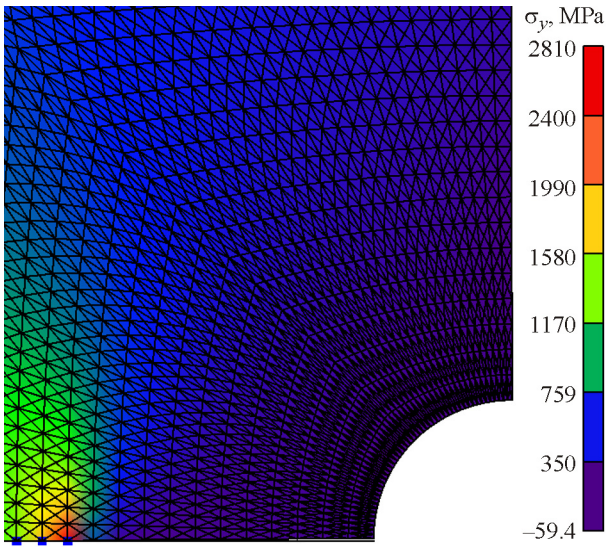

Fig. 7. Field of elastic stresses σ_y when a crack is halfway through the specimen thickness (color online).

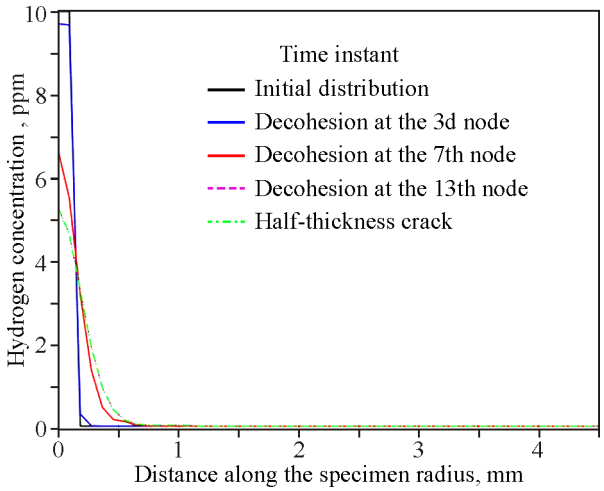

Fig. 8. Hydrogen concentration versus distance along the specimen radius (color online).

This process is observed up to the thirteenth node, which corresponds to the distance 1.102 mm from the specimen surface. The field of elastic stress distribution at this time instant is shown in Fig. 7. In this case, the critical hydrogen concentration, at which the fracture criterion is fulfilled, is $C = 0.113$ ppm.

Thereafter elastic stresses acting along the lower side of the domain become so high that the background concentration in the material is sufficient to reduce the level of cohesive stresses (according to Serebrinsky's formula (5)). Therefore, when solving the diffusion problem, the fracture criterion starts to fulfill already at the first time step and the hydrogen content at the node decreases progressively. For example, it is $C = 0.103$ ppm at the fourteenth node (1.194 mm from the groove surface) and $C = 0.1005$ ppm at the fifteenth node (1.286 mm from the edge).

Figure 8 shows the hydrogen concentration distribution along the specimen radius at different time instants: from the initial state to the instant when a crack passes a quarter of the specimen thickness.

Under the action of mechanical stresses, hydrogen is gradually distributed and transferred from the specimen surface to the material interior. However, one can see that it does not diffuse deeper than 1.25 mm from the surface. Further fracture of the specimen occurs already at the initial background hydrogen concentration due to high stresses acting in the region.

5. DISCUSSION

By using the HEDE model with consideration for the skin effect, we obtained the results on brittle fracture in hydrogen-charged corset specimens. The considered parameters of the specimens and loading conditions are common for hydrogen brittleness tests [61–65].

The results obtained using the HEDE model were compared with the experimental data only in terms of the incubation time of crack growth. A universal means of fitting to the experimental data is the initial hydrogen concentration, which is considered by all authors to be uniform. Such fitting gives its wide scatter in different papers. Sometimes it differs by several orders of magnitude from the experimental average hydrogen concentration. We took experimentally measured values of concentration after 96 h of hydrogen charging of specimens [17–20].

We found that the incubation time of the macrocrack growth is determined not by the time of increase of hydrogen concentration at the crack tip from the uniform one, but by the diffusion time of the increased hydrogen concentration from the skin layer to the crack tip. A microcrack in the skin layer is formed immediately after the application of a mechanical load. This also agrees with the numerous experimental data on the formation of microscopic quasi-cleavage cracks on the surface of hydrogen-charged specimens under deformation.

From a mechanical point of view (excluding hydrogen), the HEDE model is linear and less accurate than modern approaches that take into account the size and configuration of grains, plasticity, and other nonlinear effects, including the reciprocal influence in the crack ensemble. At the same time, the model is generally recognized in modeling of hydrogen brittleness and allows us to investigate the skin effect in the simplest approximation, without any additional assumptions.

In our modeling, we used hydrogen diffusion Eq. (2). It ignores the presence of hydrogen traps [66] inside the material. All hydrogen is thought to be in the perfect crystal lattice. On the one hand, this is undoubtedly a simplifying assumption; on the other hand, it allows one to estimate the net effect of the skin layer formed during hydrogen charging of corset specimens. At the same time, such an assumption is physically possible; we simply assume a defect-free (without trap sites) homogeneous internal structure in the specimen.

There is another factor that justifies the made assumptions. According to the Oriani trap model for hydrogen transport in metals [66], the binding energy of trapped hydrogen is much higher than the diffusion activation energy, and the volume concentration

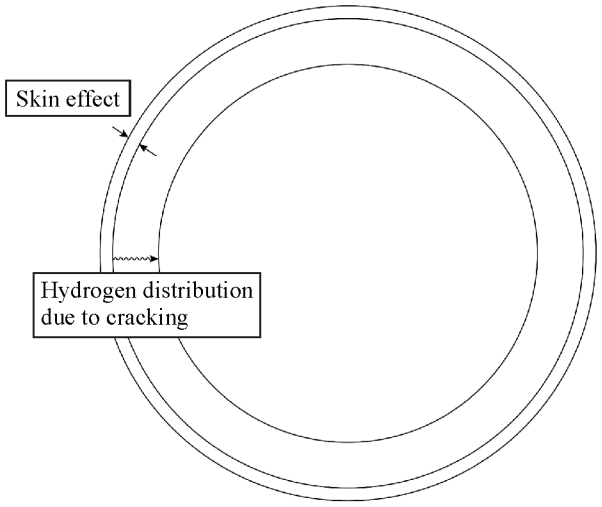

Fig. 9. Schematic of the regions of propagation of hydrogen and conventional cracks at the fracture surface.

of trapped hydrogen is only a fraction of the concentration of hydrogen diffusing in the crystal lattice. Otherwise the Oriani formula relating trapped hydrogen to lattice one does not work. This is because it is unclear from where hydrogen can be obtained with a sharp change in the volume concentration of trapping sites (such a change occurs, for example, during plastic deformation and this is one of the problems of the HELP model). Oriani's assumptions make the effect of trapped hydrogen insignificant in dynamic processes since it has a smaller concentration and redistributes much more slowly than mobile hydrogen. Naturally, Oriani himself and his followers proceeded from the fact that the processes of hydrogen redistribution are slow and the entire system at each step must be in thermodynamic equilibrium. This raises the question of whether these assumptions are adequate to conditions of strength tests on notched and grooved corset specimens [38, 40, 67–70].

We found out that the experimentally discovered skin effect leads to a dual mechanism of fracture. We can schematically represent the following distribution of the areas of influence of hydrogen over the cross section of the specimen (Fig. 9).

We understand that our calculation of crack propagation is rather simplified. As a rule, the HEDE model is used to calculate the moment of growth of a hydrogen-induced crack. Theoretically, the maximum mechanical stresses at the tip of a crack of a certain length are unbounded. Therefore, stress values obtained by the finite volume method for corner nodes can only be considered as a kind of approximation. The use of the HEDE model to describe the crack propagation in a metal free of hydrogen is also the very first rough approximation.

In our opinion, the most important result is the description of the influence of the skin effect in hydrogen-charged specimens on the HEDE mechanism. We found that a crack is quickly initiated, but it has a microscopic length for a long time since its growth is limited by hydrogen redistribution due to diffusion. This diffusion motion occurs simultaneously with a decrease in the hydrogen concentration around the crack and stops its growth by the brittle mechanism. Moreover, the mechanism of hydrogen-induced, brittle, fracture acts much deeper than the initial thickness of the hydrogen-saturated skin layer. At the edges of the fracture surface, brittle fracture is associated with an increased hydrogen concentration. Areas of hydrogen brittleness should be observed in this part of the specimen. The middle part exhibits usual fracture by the decohesion mechanism. This duality was often found in experiments [63, 71]. Moreover, an annular crack similar to that in Fig. 9 with the characteristic width about 1 mm was obtained on grooved corset cylindrical steel specimens [63].

The dual pattern of fracture is usually explained by the two main mechanisms of hydrogen-induced degradation of metals: the HEDE and HELP mechanisms. It should be noted that the HEDE mechanism was initially considered as a mechanism of pure brittle fracture, but later, by formally combining the HEDE model with the elastic-plastic material model, this rigorous approach began to "smear" [72–74].

The HELP + HEDE model of hydrogen brittleness has been recently used to describe the duality of hydrogen-induced fracture observed in practice. Thus, fracture is described either by the HELP mechanism which provides hydrogen-induced plastic fracture or by the brittle HEDE mechanism, depending on the local concentration of hydrogen at the crack tip [67, 75, 76].

According to [24, 38, 41, 77–79], the HELP mechanism works at the hydrogen concentration below the threshold C_{H0}, whereas the HEDE mechanism activates at the C_{Hcr} concentration. These assumptions were used to make approximations of the experimental data and to plot the distribution of hydrogen over the cross section of a specimen based on the fracture pattern. However, this hybrid concept does not deal with direct measurements of the distribution of hydrogen concentration. It focuses only on the microstructure of the fracture surface.

Almost all publications on the HELP and HEDE models use the assumption of the initially uniform

hydrogen concentration. The presence of such inconsistencies in the known approaches allows us to say that the nonuniform hydrogen distribution in hydrogen-charged specimens is the true reason for the dual pattern of fracture observed in practice.

When verifying the models, many authors take the hydrogen concentration values calculated by Taha and Sofronis [80] as the reference data. These values indicate that the hydrogen concentration at the crack tip exceeds manifold the average values. This excess is obtained due to the formation of a large number of hydrogen sites inside dislocations during plastic deformation. The calculations performed by the authors of the HELP model in [44] show that significant changes in the mechanical properties of a metal occur at local relative mass hydrogen concentrations of about 10^{-2}, which is an unattainable concentration for most metals. The calculation of local plasticity in the theoretical analysis of a crack with a spherical tip showed that the local hydrogen concentration at the crack tip is about 100 times higher than the average one [69]. Given the average mass concentration of about 10^{-6}, local concentrations do not exceed 10^{-4}. Thus, the assumption about the operation of the HELP mechanism at low average hydrogen concentrations does not correspond to the verification results. At low average hydrogen concentrations, external mechanical stresses cannot induce such local hydrogen accumulation that can trigger the physical mechanisms of hydrogen-enhanced localized plasticity.

This is especially important for industrial tests for hydrogen-induced cracking of metals based on the methods of hydrogen charging of specimens resulting in the skin effect. It is necessary to additionally investigate whether this effect occurs when oil, gas, hydrogen or other aggressive mixtures are pumped through pipelines and how it affects mechanic stresses in pipe walls.

6. CONCLUSIONS

We carried out special finite volume modeling of fracture of a hydrogen-charged corset cylindrical steel specimen with a notch. The HEDE model was used as a model of hydrogen embrittlement. The experimentally observed skin effect due to hydrogen charging was taken into account.

The simulation results demonstrated that fracture begins from the specimen surface as brittle fracture induced by hydrogen, then, due to the "lag" of diffusion fluxes of hydrogen, the crack grows by itself at normal background values of the hydrogen concentration.

This results in a dual pattern of fracture. The areas of both hydrogen embrittlement and normal fracture are observed on the fracture surface of the specimen.

The nonuniform distribution of hydrogen concentration can be the main source of the dual pattern of fracture, which is currently explained by the simultaneous operation of the HELP and HEDE mechanisms at the top of the main crack.

The skin effect in hydrogen-charged specimens has a strong influence on the fracture of metal specimens in spite of the very shallow depth.

Artificial charging with hydrogen can differ significantly in the distribution of hydrogen concentrations from natural saturation with hydrogen during operation, which must be taken into account in experiments since the skin effect strongly affects the results of mechanical tests.

From an engineering point of view, the obtained results mean that standard tests for hydrogen-induced cracking must be changed since the HIC due to the skin effect may not correspond to the HIC with a more uniform distribution of hydrogen inside the metal.

FUNDING

The work was performed at the Institute for Problems in Mechanical Engineering (IPME RAS) and is supported solely by the Russian Science Foundation (Grant No. 18-19-00160).

REFERENCES

1. Askari, M., Aliofkhazraei, M., and Afroukhteh, S., A Comprehensive Review on Internal Corrosion and Cracking of Oil and Gas Pipelines, *J. Nat. Gas Sci. Eng*., 2019, vol. 71, p. 102971. https://doi.org/10.1016/j.jngse.2019.102971
2. Maruschak, P.O., Panin, S.V., Chausov, M.G., Bishchak, R.T., and Polyvana, U.V., Effect of Long-Term Operation on Steels of Main Gas Pipeline. Reduction of Static Fracture Toughness, *J. Nat. Gas Sci. Eng*., 2017, vol. 38, pp. 182–186. https://doi.org/10.1016/j.jngse.2016.12.015
3. Hafsi, Z., Elaoud, S., and Mishra, M., A Computational Modelling of Natural Gas Flow in Looped Network: Effect of Upstream Hydrogen Injection on the Structural Integrity of Gas Pipelines, *J. Nat. Gas Sci. Eng*., 2019, vol. 64, pp. 107–117. https://doi.org/10.1016/j.jngse.2019.01.021
4. Ishaq, H. and Dincer, I., A Comprehensive Study on Using New Hydrogen–Natural Gas And Ammonia–Natural Gas Blends for Better Performance, *J. Nat.*

Gas Sci. Eng., 2020, vol. 81, p. 103362. https://doi.org/10.1016/j.jngse.2020.103362

5. Ishaq, H. and Dincer, I., Performance Investigation of Adding Clean Hydrogen to Natural Gas for Better Sustainability, *J. Nat. Gas Sci. Eng*., 2020, vol. 78, p. 103236. https://doi.org/10.1016/j.jngse.2020.103236
6. Ozturk, M. and Dincer, I., Development of Renewable Energy System Integrated with Hydrogen and Natural Gas Subsystems for Cleaner Combustion, *J. Nat. Gas Sci. Eng*., 2020, vol. 83, p. 103583. https://doi.org/10.1016/j.jngse.2020.103583
7. Peng, D.D., Fowler, M., Elkamel, A., Almansoori, A., and Walker, S.B., Enabling Utility-Scale Electrical Energy Storage by a Power-to-Gas Energy Hub and Underground Storage of Hydrogen and Natural Gas, *J. Nat. Gas Sci. Eng*., 2016, vol. 35, pp. 1180–1199. https://doi.org/10.1016/j.jngse.2016.09.045
8. Meng, B., Gu, Ch., Zhang, L., Zhou, Ch., Li, X., Zhao, Y., Zheng, J., Chen, X., and Han, Y., Hydrogen Effects on X80 Pipeline Steel in High-Pressure Natural Gas/Hydrogen Mixtures, *Int. J. Hydrogen Energy*, 2017, vol. 42(11), pp. 7404–7412. https://doi.org/10.1016/j.ijhydene.2016.05.145
9. Nguyen, T.T., Park, J., Kim, W.S., Nahm, S.H., and Beak, U.B., Effect of Low Partial Hydrogen in a Mixture with Methane on the Mechanical Properties of X70 Pipeline Steel, *Int. J. Hydrogen Energy*, 2020, vol. 45(3), pp. 2368–2381. https://doi.org/10.1016/j.ijhydene.2019.11.013
10. Nguyen, T.T., Tak, N., Park, J., Nahm, S.H., and Beak, U.B., Hydrogen Embrittlement Susceptibility of X70 Pipeline Steel Weld under a Low Partial Hydrogen Environment, *Int. J. Hydrogen Energy*, 2020, vol. 45(43), pp. 23739–23753. https://doi.org/10.1016/j.ijhydene.2020.06.199
11. Shang, J., Zheng, J., Hua, Zh., Li, Y., Gu, Ch., Cui, T., and Meng, B., Effects of Stress Concentration on the Mechanical Properties of X70 in High-Pressure Hydrogen-Containing Gas Mixtures, *Int. J. Hydrogen Energy*, 2020, vol. 45(52), pp. 28204–28215. https://doi.org/10.1016/j.ijhydene.2020.02.125
12. Nguyen, T.T., Park, J.S., Kim, W.S., Nahm, S.H., and Beak, U.B., Environment Hydrogen Embrittlement of Pipeline Steel X70 under Various Gas Mixture Conditions with in Situ Small Punch Tests, *Mater. Sci. Eng. A*, 2020, vol. 781, p. 139114. https://doi.org/10.1016/j.msea.2020.139114
13. ISO11114-4. Transportable Gas Cylinders—Compatibility of Cylinder and Valve Materials with Gas Contents. Part 4: Test Methods for Selecting Metallic Materials Resistant to Hydrogen Embrittlement, ISO 11114-4:2017, Int. Organization for Standardization, 2017.
14. ISO16573. Steel—Measurement Method for the Evaluation of Hydrogen Embrittlement Resistance of High Strength Steels, ISO 16573:2015, Int. Organization for Standardization, 2015.
15. ISO17081. Method of Measurement of Hydrogen Permeation and Determination of Hydrogen Uptake and Transport in Metals by an Electrochemical Technique, ISO 17081:2014, Int. Organization for Standardization, 2014.
16. TM0284. Evaluation of Pipeline and Pressure Vessel Steels for Resistance to Hydrogen-Induced Cracking. TM0284-2016 ANSI/NACE Standard, Houston, TX: NACE Int., 2016.
17. Alekseeva, E.L., Belyaev, A.K., Zegzhda, A.S., Polyanskiy, A.M., Polyanskiy, V.A., Frolova, K.P., and Yakovlev, Yu.A., Boundary Layer Influence on the Distribution of Hydrogen Concentrations during Hydrogen-Induced Cracking Test of Steels. Diagnostics, *Resource Mech. Mater. Struct*., 2018, vol. 3, p. 43. https://doi.org/10.17804/2410-9908.2018.3.043-057
18. Martinsson, Å. and Sandström, R., Hydrogen Depth Profile in Phosphorus-Doped, Oxygen–Free Copper after Cathodic Charging, *J. Mater. Sci*., 2012, vol. 47(19), pp. 6768–6776. https://doi.org/10.1007/s10853-012-6592-y
19. Polyanskiy, V.A., Belyaev, A.K., Alekseeva, E.L., Polyanskiy, A.M., Tretyakov, D.A., and Yakovlev, Yu.A., Phenomenon of Skin Effect in Metals due to Hydrogen Absorption, *Continuum Mech. Thermodyn*., 2019, vol. 31(6), pp. 1961–1975. https://doi.org/10.1007/s00161-019-00839-2
20. Wu, T.-I. and Wu, J.-Ch., Effects of Cathodic Charging and Subsequent Solution Treating Parameters On The Hydrogen Redistribution And Surface Hardening of Ti–6Al–4V Alloy, *J. Alloy. Compnd*, 2008, vol. 466(1), pp. 153–159. https://doi.org/10.1016/j.jallcom.2007.11.045
21. Frolova, K.P., Vilchevskaya, E.N., Polyanskiy, V.A., and Yakovlev, Yu.A., Modeling the Skin Effect Associated with Hydrogen Accumulation by Means of the Micropolar Continuum, *Continuum Mech. Thermodyn*., 2021, vol. 33(3), pp. 697–711. https://doi.org/10.1007/s00161-020-00948-3
22. Hadam, U. and Zakroczymski, T., Absorption of Hydrogen in Tensile Strained Iron and High-Carbon Steel Studied by Electrochemical Permeation and Desorption Techniques, *Int. J. Hydrogen Energy*, 2009, vol. 34(5), pp. 2449–2459. https://doi.org/10.1016/j.ijhydene.2008.12.088
23. Omura, T., Nakamura, J., Hirata, H., Jotoku, K., Ueyama, M., Osuki, T., and Terunuma, M., Effect of Surface Hydrogen Concentration on Hydrogen Embrittlement Properties of Stainless Steels and Ni Based Alloys, *ISIJ Int*., 2016, vol. 56(3), pp. 405–412. https://doi.org/10.2355/isijinternational.ISIJINT-2015-268
24. Djukic, M.B., Bakic, G.M., Zeravcic, V.S., Sedmak, A., and Rajicic, B., The Synergistic Action and Interplay of Hydrogen Embrittlement Mechanisms in Steels and Iron: Localized Plasticity and Decohesion, *Eng. Fract. Mech*., 2019, vol. 216, p. 106528. https://doi.org/10.1016/j.engfracmech.2019.106528

25. Lynch, S., Hydrogen Embrittlement Phenomena and Mechanisms, *Corrosion Rev*., 2012, vol. 30(3-4), pp. 105–123. https://doi.org/10.1515/corrrev-2012-0502
26. Oriani, R.A., A Mechanistic Theory of Hydrogen Embrittlement of Steels, *Berichte der Bunsengesellschaft für physikalische Chem*., 1972, vol. 76(8), pp. 848–857. https://doi.org/10.1002/bbpc.19720760864
27. Birnbaum, H.K. and Sofronis, P., Hydrogen-Enhanced Localized Plasticity—Mechanism for Hydrogen-Related Fracture, *Mater. Sci. Eng. A*, 1994, vol. 176(1), pp. 191–202. https://doi.org/10.1016/0921-5093(94)90975-X
28. Sofronis, P. and Birnbaum, H.K., Mechanics of the Hydrogen-Dislocation-Impurity Interactions—I. Increasing Shear Modulus, *J. Mech. Phys. Solids*, 1995, vol. 43(1), pp. 49–90. https://doi.org/10.1016/0022-5096(94)00056-B
29. Beachem, C.D., A New Model for Hydrogen-Assisted Cracking (Hydrogen "Embrittlement"), *Metall. Mater. Trans. B*, 1972, vol. 3(2), pp. 441–455. https://doi.org/10.1007/BF02642048
30. Bond, G.M., Robertson, I.M., and Birnbaum, H.K., The Influence of Hydrogen on Deformation and Fracture Processes in High-Strength Aluminum Alloys, *Acta Metall*., 1987, vol. 35(9), pp. 2289–2296. https://doi.org/10.1016/0001-6160(87)90076-9
31. Ferreira, P.J., Robertson, I.M., and Birnbaum, H.K., Hydrogen Effects on the Interaction between Dislocations, *Acta Mater*., 1998, vol. 46(5), pp. 1749–1757. https://doi.org/10.1016/S1359-6454(97)00349-2
32. Ferreira, P.J., Robertson, I.M., and Birnbaum, H.K., Hydrogen Effects on the Character of Dislocations in High-Purity Aluminum, *Acta Mater*., 1999, vol. 47(10), pp. 2991–2998. https://doi.org/10.1016/S1359-6454(99)00156-1
33. Li, Y., Gong, B., Li, X., Deng, C., and Wang, D., Specimen Thickness Effect on the Property of Hydrogen Embrittlement in Single Edge Notch Tension Testing of High Strength Pipeline Steel, *Int. J. Hydrogen Energy*, 2018, vol. 43(32), pp. 15575–15585. https://doi.org/10.1016/j.ijhydene.2018.06.118
34. Robertson, I.M. and Birnbaum, H.K., An HVEM Study of Hydrogen Effects on the Deformation and Fracture of Nickel, *Acta Metall*., 1986, vol. 34(3), pp. 353–366. https://doi.org/10.1016/0001-6160(86)90071-4
35. Robertson, I.M., Birnbaum, H.K., Heubaum, F., Tabata, T., and Wei, W., Hydrogen Embrittlement and Grain Boundary Fracture, *Scripta Metall*., 1984, vol. 18(8), p. 8.
36. Gerberich, W., Modeling Hydrogen Induced Damage Mechanisms in Metals, in *Metals and Surface Engineering. V. 1. Gaseous Hydrogen Embrittlement of Materials in Energy Technologies*, Gangloff, R.P. and Somerday, B.P., Eds., Woodhead Publ., 2012, pp. 209–246. https://doi.org/10.1533/9780857095374.2.209
37. Martin, M.L., Dadfarnia, M., Nagao, A., Wang, Sh., and Sofronis, P., Enumeration of the Hydrogen-Enhanced Localized Plasticity Mechanism for Hydrogen Embrittlement in Structural Materials, *Acta Mater*., 2019, vol. 165, pp. 734–750. https://doi.org/10.1016/j.actamat.2018.12.014
38. Djukic, M.B., Sijacki Zeravcic, V., Bakic, G., Sedmak, A., and Rajicic, B., Hydrogen Embrittlement of Low Carbon Structural Steel, *Proc. Mater. Sci*., 2014, vol. 3, pp. 1167–1172. https://doi.org/10.1016/j.mspro.2014.06.190
39. Gerberich, W.W., Stauffer, D.D., and Sofronis, P., A Coexistent View of Hydrogen Effects on Mechanical Behavior of Crystals: HELP and HEDE, in *Effects of Hydrogen on Materials*, Materials Park, OH: ASM Int., 2009, pp. 38–45.
40. Singh, R., Singh, V., Arora, A., and Mahajan, D.K., In-situ Investigations of Hydrogen Influenced Crack Initiation and Propagation under Tensile and Low Cycle Fatigue Loadings in RPV Steel, *J. Nucl. Mater*., 2020, vol. 529, p. 151912.
41. Wasim, M., Djukic, M.B., and Ngo, T.D., Influence of Hydrogen-Enhanced Plasticity and Decohesion Mechanisms of Hydrogen Embrittlement on the Fracture Resistance of Steel, *Eng. Failure Analysis*, 2021, vol. 123, p. 105312. https://doi.org/10.1016/j.engfailanal.2021.105312
42. Falkenberg, R., Brocks, W., Dietzel, W., and Scheider, I., Modelling the Effect of Hydrogen on Ductile Tearing Resistance of Steels, *Int. J. Mater. Res*., 2010, vol. 101(8), pp. 989–996. https://doi.org/10.3139/146.110368
43. Sobotka, J.C., Dodds, R.H., and Sofronis, P., Effects of Hydrogen on Steady, Ductile Crack Growth: Computational Studies, *Int. J. Solids Struct*., 2009, vol. 46(22), pp. 4095–4106. https://doi.org/10.1016/j.ijsolstr.2009.08.002
44. Sofronis, P., Liang, Y., and Aravas, N., Hydrogen Induced Shear Localization of the Plastic Flow in Metals and Alloys, *Eur. J. Mech. A. Solids*, 2001, vol. 20(6), pp. 857–872. https://doi.org/10.1016/S0997-7538(01)01179-2
45. Liang, Y., Ahn, D.C., Sofronis, P., Dodds, R.H., and Bammann, D., Effect of Hydrogen Trapping on Void Growth and Coalescence in Metals and Alloys, *Mech. Mater*., 2008, vol. 40(3), pp. 115–132. https://doi.org/10.1016/j.mechmat.2007.07.001
46. Liang, Y. and Sofronis, P., Toward a Phenomenological Description of Hydrogen-Induced Decohesion at Particle/Matrix Interfaces, *J. Mech. Phys. Solids*, 2003, vol. 51(8), pp. 1509–1531. https://doi.org/10.1016/S0022-5096(03)00052-8
47. Liang, Y. and Sofronis, P., On Hydrogen-Induced Void Nucleation and Grain Boundary Decohesion in Nickel-Base Alloys, *J. Eng. Mater. Technol*., 2004, vol. 126(4), pp. 368–377. https://doi.org/10.1115/1.1789954

48. Jemblie, L., Olden, V., Maincon, P., and Akselsen, O.M., Cohesive Zone Modelling of Hydrogen Induced Cracking on the Interface of Clad Steel Pipes, *Int. J. Hydrogen Energy*, 2017, vol. 42(47), pp. 28622–28634. https://doi.org/10.1016/j.ijhydene.2017.09.051
49. Vergani, L., Gobbi, G., and Colombo, Ch., A Numerical Model to Study the Hydrogen Embrittlement Effect on Low-Alloy Steels, *Key Eng. Mater*., 2014, vol. 577, pp. 513–516. https://doi.org/10.4028/www.scientific.net/KEM.577-578.513
50. Shewmon, P., *Diffusion in Solids*, Springer, 2016.
51. Gorsky, W.S., Theorie der elastischen Nachwirkung in ungeordneten Mischkristallen (elastische Nachwirkung zweiter Art), *Physikalische Zeitschrift der Sowjetunion*, 1935, vol. 8, pp. 457–471.
52. Serebrinsky, S., Carter, E.A., and Ortiz, M., A Quantum-Mechanically Informed Continuum Model of Hydrogen Embrittlement, *J. Mech. Phys. Solids*, 2004, vol. 52(10), pp. 2403–2430. https://doi.org/10.1016/j.jmps.2004.02.010
53. McLean, D., *Grain Boundaries in Metals*, Clarendon Press, 1957.
54. Hirth, J.P., Effects of Hydrogen on the Properties of Iron and Steel, *Met. Trans. A*, 1980, vol. 11(6), pp. 861–890. https://doi.org/10.1007/BF02654700
55. Wilkins, M.L., *Calculation of Elastic-Plastic Flow: Technical Report*, California Univ. Livermore Radiation Lab., 1963.
56. Wilkins, M.L., *Computer Simulation of Dynamic Phenomena*, Berlin: Springer-Verlag, 1999.
57. Tvergaard, V. and Hutchinson, J.W., The Relation Between Crack Growth Resistance and Fracture Process Parameters in Elastic-Plastic Solids, *J. Mech. Phys. Solids*, 1992, vol. 40(6), pp. 1377–1397. https://doi.org/10.1016/0022-5096(92)90020-3
58. Bessonov, N.M., Golovashchenko, S.F., and Volpert, V.A., Numerical Modelling of Contact Elastic-Plastic Flows, *Math. Model. Nat. Phenomen*., 2009, vol. 4(1), pp. 44–87. https://doi.org/10.1051/mmnp/20094103
59. Golovashchenko, S.F., Bessonov, N.M., and Ilinich, A.M., Two-Step Method of Forming Complex Shapes from Sheet Metal, *J. Mater. Proc. Technol*., 2011, vol. 211(5), pp. 875–885. https://doi.org/10.1016/j.jmatprotec.2010.01.004
60. Polyanskiy, V.A., Belyaev, A.K., Chevrychkina, A.A., Varshavchik, E.A., and Yakovlev, Yu.A., Impact of Skin Effect of Hydrogen Charging on the Choo-Lee Plot for Cylindrical Samples, *Int. J. Hydrogen Energy*, 2021, vol. 46(9), pp. 6979–6991. https://doi.org/10.1016/j.ijhydene.2020.11.192
61. Hui, W., Xu, Zh., Zhang, Yo., Zhao, X., Shao, Ch., and Weng, Yu., Hydrogen Embrittlement Behavior of High Strength Rail Steels: A Comparison between Pearlitic and Bainitic Microstructures, *Mater. Sci. Eng. A*, 2017, vol. 704, pp. 199–206. https://doi.org/10.1016/j.msea.2017.08.022
62. Lin, Yu-Ch., Chen, D., Chiang, M.H., Cheng, G.-J., Lin, H.-Ch., and Yen, H.W., Response of Hydrogen Desorption and Hydrogen Embrittlement to Precipitation of Nanometer-Sized Copper in Tempered Martensitic Low-Carbon Steel, *JOM*, 2019, vol. 71(4), pp. 1349–1356. https://doi.org/10.1007/s11837-019-03330-0
63. Peral, L.B., Zafra, A., Fernandez-Pariente, I., Rodriguez, C., and Belzunce, J., Effect of Internal Hydrogen on the Tensile Properties of Different CrMo(V) Steel Grades: Influence of Vanadium Addition on Hydrogen Trapping and Diffusion, *Int. J. Hydrogen Energy*, 2020, vol. 45(41), pp. 22054–22079. https://doi.org/10.1016/j.ijhydene.2020.05.228
64. Shibata, A., Madi, Y., Okada, K., Tsuji, N., and Besson, J., Mechanical and Microstructural Analysis on Hydrogen-Related Fracture in a Martensitic Steel, *Int. J. Hydrogen Energy*, 2019, vol. 44(54), pp. 29034–29046. https://doi.org/10.1016/j.ijhydene.2019.09.097
65. Wang, M., Akiyama, E., and Tsuzaki, K., Effect of Hydrogen and Stress Concentration on the Notch Tensile Strength of AISI 4135 Steel, *Mater. Sci. Eng. A*, 2005, vol. 398(1), pp. 37–46. https://doi.org/10.1016/j.msea.2005.03.008
66. Oriani, R.A., The Diffusion and Trapping of Hydrogen In Steel, *Acta Metall*., 1970, vol. 18(1), pp. 147–157. https://doi.org/10.1016/0001-6160(70)90078-7
67. Asadipoor, M., Kadkhodapour, J., Pourkamali Anaraki, A., Sharifi, S.M.H., Darabi, A.Ch., and Barnoush, A., Experimental and Numerical Investigation of Hydrogen Embrittlement Effect on Microdamage Evolution of Advanced High-Strength Dual-Phase Steel, *Met. Mater. Int*., 2021, vol. 27, pp. 2276–2291. https://doi.org/10.1007/s12540-020-00681-1
68. Bal, B., Okdem, B., Bayram, F.C., and Aydin, M., A Detailed Investigation of the Effect of Hydrogen on the Mechanical Response and Microstructure of Al 7075 Alloy under Medium Strain Rate Impact Loading, *Int. J. Hydrogen Energy*, 2020, vol. 45(46), pp. 25509–25522. https://doi.org/10.1016/j.ijhydene.2020.06.241
69. Singh, R., Singh, A., Singh, P.K., and Mahajan, D.K., Role of Prior Austenite Grain Boundaries in Short Fatigue Crack Growth in Hydrogen Charged RPV Steel, *Int. J. Pressure Vessels Piping*, 2019, vol. 171, pp. 242–252. https://doi.org/10.1016/j.jnucmat.2019.151912
70. Toribio, J., HELP versus HEDE in Progressively Cold-Drawn Pearlitic Steels: Between Donatello and Michelangelo, *Eng. Failure Analysis*, 2018, vol. 94, pp. 157–164. https://doi.org/10.1016/j.engfailanal.2018.07.026
71. Venezuela, J., Hill, T., Zhou, Q., Li, H., Shi, Zh., Dong, F., Knibbe, R., Zhang, M., Dargusch, M.S., and Atrens, A., Hydrogen-Induced Fast Fracture in Notched 1500 and 1700 MPa Class Automotive Martensitic Advanced High-Strength Steel, *Corrosion Sci*.,

2021, vol. 188, p. 109550. https://doi.org/10.1016/j.corsci.2021.109550
72. Birnbaum, H.K., Hydrogen Effects on Deformation and Fracture: Science and Sociology, *MRS Bullet*., 2003, vol. 28(7), pp. 479–485. https://doi.org/10.1557/mrs2003.143
73. Martin, M.L., Fenske, J.A., Liu, G.S., Sofronis, P., and Robertson, I.M., On the Formation and Nature of Quasi-Cleavage Fracture Surfaces on Hydrogen Embrittled Steels, *Acta Mater*., 2011, vol. 59(4), pp. 1601–1606. https://doi.org/10.1016/j.actamat.2010.11.024
74. Singh, D.K., Maiti, S.K., Bhandakkar, T.K., and Singh Raman, R.K., Efficient Approach for Cohesive Zone Based Three-Dimensional Analysis of Hydrogen-Assisted Cracking of a Circumferentially Notched Round Tensile Specimen, *Int. J. Hydrogen Energy*, 2017, vol. 42(24), pp. 15943–15955. https://doi.org/10.1016/j.ijhydene.2017.05.064
75. Elmukashfi, E., Tarleton, E., and Cocks, A.C.F., A Modelling Framework for Coupled Hydrogen Diffusion and Mechanical Behaviour of Engineering Components, *Comput. Mech*., 2020, vol. 66, pp. 189–220. https://doi.org/10.1007/s00466-020-01847-9
76. Huang, C. and Gao, X., Phase Field Modeling of Hydrogen Embrittlement, *Int. J. Hydrogen Energy*, 2020, vol. 45(38), pp. 20053–20068. https://doi.org/10.1016/j.ijhydene.2020.05.015
77. Djukic, M.B., Sijacki Zeravcic, V., Bakic, G.M., Sedmak, A., and Rajicic, B., Hydrogen Damage of Steels: A Case Study and Hydrogen Embrittlement Model, *Eng. Failure Analysis*, 2015, vol. 58, pp. 485–498.
78. Djukic, M.B., Bakic, G.M., Zeravcic, V.S., Sedmak, A., and Rajicic, B., Hydrogen Embrittlement of Industrial Components: Prediction, Prevention, and Models, *Corrosion*, 2016, vol. 72(7), pp. 943–961. https://doi.org/10.5006/1958
79. Wasim, M. and Djukic, M.B., Hydrogen Embrittlement of Low Carbon Structural Steel at Macro-, Micro- and Nano-Levels, *Int. J. Hydrogen Energy*, 2020, vol. 45(3), pp. 2145–2156. https://doi.org/10.1016/j.ijhydene.2019.11.070
80. Taha, A. and Sofronis, P., A Micromechanics Approach to the Study of Hydrogen Transport and Embrittlement, *Eng. Fract. Mech*., 2001, vol. 68(6), pp. 803–837. https://doi.org/10.1016/S0013-7944(00)00126-0